Dynamical and Voltage Profile Stability of Inverter-Connected Distributed Power Generation

Chung-Ching Chang, *Student Member, IEEE,* Dimitry Gorinevsky, *Fellow, IEEE,* and Sanjay Lall, *Senior Member, IEEE*

***Abstract*—We present a systematic stability analysis of inverter-connected distributed generation. Our approach is to replace simulations with much faster and more informative analysis using transfer functions. The transfer functions characterize the dynamics of the interconnected feedback loops in the system. The methodology is applicable to different types of inverters, including droop inverters. It also may be applied to distribution systems with arbitrary topology. The analysis allows evaluation of system stability and performance, subject to frequency, load, and power set-point disturbances. By means of two examples we demonstrate how the proposed approach can help in analysis and engineering of the distribution systems with acceptable frequency and voltage profile responses to both distributed generation power and grid frequency disturbances.**

***Index Terms*—Distributed power generation, power distribution, power system stability, power system control, inverters.**

I. Introduction

THE integration of renewable energy sources is a substantial change to the electricity distribution system and the control systems in the power grid. This paper describes an approach for determining whether the resulting interaction of distributed feedback loops can produce system instability or sensitivity to disturbances.

The existing electrical grid was designed for centralized power generation. Bulk power supply and demand are balanced by the rotational energy of multi-ton rotors of synchronous generators. When load suddenly increases, it drains power through the distribution system, transmission system, and finally from the rotors. As a result, the frequency of the grid decreases. This effect is called frequency droop. On the distribution side, the unidirectional power flow from feeder to end customers defines the voltage profile over a line.

Distribution systems with distributed renewable energy sources change this paradigm. Solar, wind, and other sources are connected through inverters that transform direct current (DC) to alternating current (AC). Inverters can use droop control logic to emulate the stabilizing effect of rotational inertia. Such droop inverters interact through line frequency changes, and can provide some amount of balancing of the distributed power generation.

This paper analyzes dynamics of the interconnected feedback loops that result when using droop inverters. The question of how exogenous disturbances propagate is addressed. In particular a question is whether frequency disturbances in the bulk power system can amplify and trip the protections of the distribution system. The paper also considers how voltage profiles might be affected by environment condition changes to solar panel or wind turbine power production.

The analysis of bulk generation and transmission of electrical power has been developed over several decades. The established approaches include small-signal linear perturbation models of such systems [1] and nonlinear model simulations.

The corresponding analysis for distribution systems with inverter connected generation is less developed. Most of the prior work is on simulating specific systems, e.g., see [2]. The related analytical studies consider distribution systems with a single inverter or two parallel connected inverters in a microgrid. The inverters are modeled as ideal voltage sources, possibly coupled to the grid through an output impedance, see [3]–[8]. These idealized models ignore the transient dynamics, which often dominate the inverter systems.

The small signal analysis of the transient dynamics for microgrids with multiple inverters includes [9]–[14]. These papers model inverter dynamics including voltage/current acuation control logic as well as the inverter output filter circuit. In [9], [10], the objective is to tune droop controller gain. Dynamic stability and load sharing for droop control are analyzed in [11]–[13]. An enhancement of droop control by introducing communications between inverters is considered in [14]. All of these papers consider stability of transient dynamics of parallel inverters in a microgrid.

There is little prior work in small signal analysis of the transient dynamics for *grid-connected* distribution systems with inverter connected generation. The existing papers [3], [6], [9], [11], [12] analyze power sharing, but not the resulting effect on voltage profile. Frequency stability and voltage profile are simulated in [2] without further analysis. Frequency and voltage are analyzed in [3] using simplified inverter model. The only detailed analysis known to the authors is [15], where a single grid-tie inverter is considered as a lumped model of the distributed generation.

The contribution of this paper is in the methodology of small-signal modeling and transient dynamics analysis for grid-connected distribution systems with multiple inverter-connected generators. We use more comprehensive models than those in the prior literature, including inverter measurements, actuation, and exogenous disturbances. We construct system transfer functions and show examples of their use for engineering analysis. This paper details results for droop inverters in a linear topology circuit. However, the analysis

C.-C. Chang, D. Gorinevsky, and S. Lall are with the Department of Electrical Engineering, Stanford University, Stanford, CA 94305, USA (e-mall: {bobbyc, gorin, lall}@stanford.edu

This work was supported by the TomKat Center for Sustainable Energy Seed Grant “Analysis and Control of Smart Electrical Distribution Systems”

methodology can be extended to other types of inverters and distribution circuit topologies.

We consider example problems in single and multiple inverter tuning and in voltage profile analysis. Our analysis approach can also be useful for distribution management systems [16], voltage profile management, Volt-Var optimization, load balancing, and contingency analysis.

The paper is organized as follows. The system model is introduced in Section II and then detailed for droop inverters. Models of a single inverter system are formulated in Section III and of multiple inverter systems in Section IV. The models are used to characterize system performance in terms of disturbance rejection. Finally, Section V presents two examples that use small signal transfer functions in engineering analysis of distribution systems.

II. Droop Control

This section introduces the notation, the circuit model, and the droop inverter logic. The inverter models are considered in the following sections.

A. Dynamic Phasors

Throughout this paper, we describe grid voltage V_G, grid current I_G, inverter voltage V_N, inverter current I_N, and load current I_L by root-mean-square (RMS) phasors, complex variables. The phasors describe amplitudes and phases of the underlying AC signals with baseline frequency f_0 (60Hz in US). A phasor can be represented in two different ways. For example, the voltage V_N may be represented by

- a single complex variable $V_N = \Re V_N + i\Im V_N$ where $\Re$ and $\Im$ denote the real and imaginary part and $i = \sqrt{-1}$;
- amplitude $|V_N|$ and phase angle ϕ_N in $V_N = |V_N|\angle\phi_N$;

The dynamic phasors are functions of time. The analysis uses linearized models of the phasor dynamics in the vicinity of the steady-state.

In the steady-state, the frequency of V_N is $f_N = f_0$. The time-varying frequency f_N is modeled through time-varying phase ϕ_N in the phasor V_N. The same representations apply to the phasor V_G.

$$\frac{d}{dt}\phi_N = 2\pi(f_N - f_0), \qquad \frac{d}{dt}\phi_G = 2\pi(f_G - f_0), \quad (1)$$

The dynamics of phasors will be described using the Laplace operator s. For example, the first equation in (1) is $\phi_N = \frac{2\pi}{s} f_N$. The time varying frequency f_G is an external disturbance in the distribution system. Finally, note that all phases in the circuits are relative. This allows one to choose a reference phase. For example, we can assume $\phi_N = 0$ or $\phi_G = 0$.

B. Model of Distribution Circuit

Figure 1 shows a simplified single-phase model of an AC distribution circuit. This is an equivalent circuit model as seen from the low voltage circuit; there is no transformer. Section IV extends this model to multiple inverters.

The modeled distribution system is connected to the grid and to a single customer. The power distribution line has

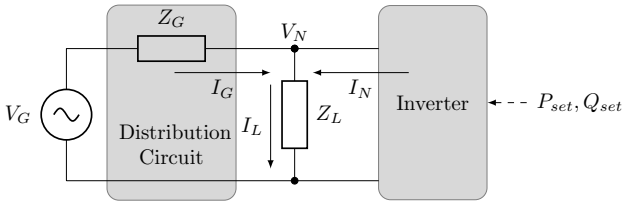

Fig. 1: Model of distribution circuit.

impedance $Z_G \in \mathbb{C}$. The grid is modeled as an ideal voltage source V_G. The customer is modeled by an aggregated load $Z_L \in \mathbb{C}$ and an inverter. Most prior work considers models similar to Figure 1, except that there is no load.

The circuit in Figure 1 follows Kirchhoff's current law (KCL), Kirchhoff's voltage law (KVL), and Ohm's law equations:

$$I_L = I_N + I_G, \quad (2)$$
$$V_G = V_N + I_G Z_G. \quad (3)$$
$$V_N = I_L Z_L \quad (4)$$

The active inverter output power $P_N \in \mathbb{R}$ and reactive power $Q_N \in \mathbb{R}$ are given by

$$P_N + iQ_N = V_N I_N^*. \quad (5)$$

Similarly, the active and reactive grid power P_G and Q_G are

$$P_G + iQ_G = V_N I_G^*. \quad (6)$$

Finally, the active and reactive load power P_L and Q_L

$$P_L + iQ_L = V_N I_L^*. \quad (7)$$

In accordance with (7), (5), (6), and (2), we also have

$$P_L + iQ_L = (P_N + iQ_N) + (P_G + iQ_G). \quad (8)$$

C. Inverter Types

This paper considers inverter control logic implementing two types of droop behavior [8].

1) Conventional Droop Inverters: These systems emulate the frequency droop seen in bulk generation and transmission. The power is balanced by adjusting the output voltage amplitude and frequency.

Suppose that Z_G is inductive, i.e. $Z_G = iX_G$ for some $X_G \in \mathbb{R}$ and set Z_L to infinity. Then according to (2), (3), and (5),

$$\begin{aligned} P_N &= \frac{|V_N||V_G|}{X_G}(\phi_N - \phi_G) \\ Q_N &= \frac{|V_N|}{X_G}(|V_N| - |V_G|) \end{aligned} \quad (9)$$

In deriving (9), we approximate $\angle(\phi_N - \phi_G) \approx 1 + i(\phi_N - \phi_G)$. This holds since $\phi_N - \phi_G$ must be small for small power dissipation in the transmission line.

The conventional droop inverters regulate the output frequency and amplitude of V_N according to

$$\begin{aligned} f_D &= f_0 - K_f(P_N - P_{set}), \\ V_D &= V_{N,0} - K_V(Q_N - Q_{set}), \end{aligned} \quad (10)$$

where $f_D \in \mathbb{R}$ and $V_D \in \mathbb{R}$ are the demand value of the frequency and amplitude of V_N, respectively, and $V_{N,0}$ is typically set to 120V. Note that (9), (10), and (1) form two separate closed-loop transfer functions: one regulates P_N through f_N and the other Q_N through $|V_N|$.

2) Opposite Droop Inverters: They emulate the droop effects taking into account inherent difference between high voltage (HV) and low voltage (LV) grids. The transmission line impedance of HV grid is mostly inductive while that of LV grid is mostly resistive. Taking $Z_G \approx R_G \in \mathbb{R}$, equations in (9) are replaced by

$$\begin{aligned} P_N &= \frac{|V_N|}{R_G}(|V_N| - |V_G|) \\ Q_N &= \frac{|V_N||V_G|}{R_G}(\phi_G - \phi_N) \end{aligned} \tag{11}$$

To reflect the resistive impedance of the LV transmission line, the opposite droop inverters follow

$$\begin{aligned} f_D &= f_0 - K_f(Q_N - Q_{set}), \\ V_D &= V_{N,0} - K_V(P_N - P_{set}). \end{aligned} \tag{12}$$

Along with (1), this forms two separate feedback loops: one regulates P_N through $|V_N|$ and the other Q_N through f_N. The opposite droop inverters are better suited for distributed generation connected to a distribution system.

D. Droop Controller Gain

An established approach to setting droop controller gains K_f and K_V is described in [17]. The approach sets largest possible gains K_f and K_V in the absolute value. The gains are defined by the frequency range $[f_{N,\min}, f_{N,\max}]$, the active power rating $[P_{N,\min}, P_{N,\max}]$, the voltage range $[|V_N|_{\min}, |V_N|_{\max}]$, and the reactive power rating $[Q_{N,\min}, Q_{N,\max}]$. In this paper, we choose the droop controller gain as follows:

$$\begin{aligned} K_f &= \min\left(\frac{f_{N,\max} - f_0}{P_{set} - P_{N,\min}}, \frac{f_0 - f_{N,\min}}{P_{N,\max} - P_{set}}\right), \\ K_V &= \min\left(\frac{|V_N|_{\max} - V_{N,0}}{Q_{set} - Q_{N,\min}}, \frac{V_{N,0} - |V_N|_{\min}}{Q_{N,\max} - Q_{set}}\right). \end{aligned}$$

For the opposite droop, we take

$$\begin{aligned} K_f &= -\min\left(\frac{f_{N,\max} - f_0}{Q_{N,\max} - Q_{set}}, \frac{f_0 - f_{N,\min}}{Q_{set} - Q_{N,\min}}\right), \\ K_V &= \min\left(\frac{|V_N|_{\max} - V_{N,0}}{P_{set} - P_{N,\min}}, \frac{V_{N,0} - |V_N|_{\min}}{P_{N,\max} - P_{set}}\right), \end{aligned}$$

where P_{set} and Q_{set} are given and the sign of K_f and K_V can be determined as shown in the example in Section V-B. Taking $\min(\cdot)$ here guarantees that the voltage and frequency are in their ranges under all load settings.

III. Model of Single Inverter

In an idealized model, the inner-loop voltage control is replaced by an ideal voltage source [3]–[8]. This replacement is justified when the inner-loop voltage control has faster response than the outer-loop droop control. Our analysis shows this is not the case. Figure 2 shows the model of the inverter with the droop control, the inverter voltage control, and the inverter circuit. We follow the design in [18].

A. Inverter System Overview

In Figure 2, the droop controller takes set-points P_{set} and Q_{set} as inputs and regulates output power P_N and Q_N by controlling output voltage V_N. The droop controller implements droop equations in Section II-C. The inverter voltage control takes the demand signals V_D and f_D from the droop controller and actuates V_N to follow these demands. It uses frequency and amplitude estimated by a phase-locked loop (PLL). The demand values f_D and V_D from the droop controller are compared to the frequency f_M and amplitude V_M of V_N estimated by the PLL. The discrepancies in frequencies and amplitudes are then fed into two proportional-integral (PI) controllers. The phase converter transforms the PI controller outputs r and θ, along with the phase of V_N measured by PLL, to a control signal V_P drives the switching of the insulated-gate bipolar transistor (IGBT) gates of the inverter. The inverter circuit is composed of IGBT switching gates followed by a lowpass LCL filter and a Δ-Y transformer.

B. System Linearization

The power distribution system normally operates close to a steady-state. Computation of steady-state for the model in Figure 2 is described in Appendix A. We consider changes of the system parameters, such as load changes, to be exogenous disturbances. The main purpose of our analysis is to see how the system responds to those disturbances.

In what follows, we form a perturbation model of the system in the vicinity of the steady-state. We first linearize each individual block shown in Figure 2, then connect the linearized blocks together to form a closed-loop transfer function. In linearizing system dynamics, the perturbations of the steady-state are denoted by δ, for example, δV_N for the transient of V_N. The perturbations, such as δV_N, are dynamic phasors, e.g. see [17]. Below we discuss the model structure. The transfer function of the linearized blocks are described in Appendix B.

C. Droop Controller

The droop controller computes P_N and Q_N from the inverter outputs V_N and I_N and generates the demand signals f_D and V_D according to the droop equations (10) or (12).

The appendix derives the measurement model

$$\begin{bmatrix} \delta P_N \\ \delta Q_N \end{bmatrix} = T_{\text{msr}} \begin{bmatrix} \Re \delta V_N \\ \Im \delta V_N \\ \Re \delta I_N \\ \Im \delta I_N \end{bmatrix}. \tag{13}$$

and the droop controller model

$$\begin{bmatrix} \delta V_D \\ \delta f_D \end{bmatrix} = T_{\text{droop}} \left(\begin{bmatrix} \delta P_N \\ \delta Q_N \end{bmatrix} - \begin{bmatrix} \delta P_{set} \\ \delta Q_{set} \end{bmatrix} \right). \tag{14}$$

D. PLL

The PLL block receives the voltage input V_N and generates unit amplitude output V_N', the measured frequency f_M, and

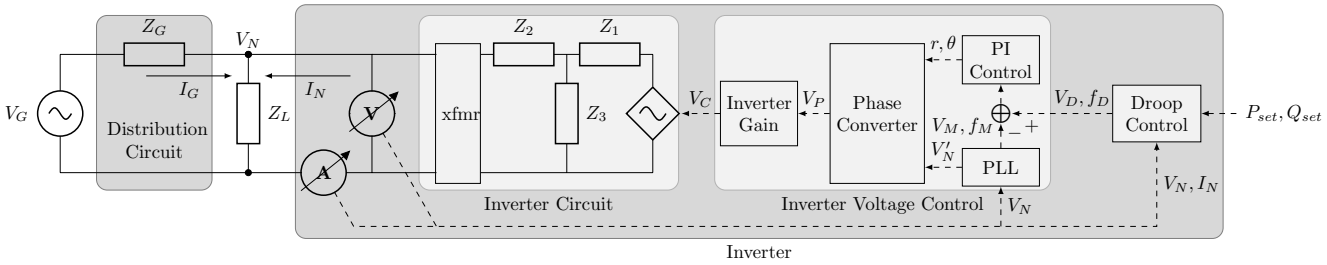

Fig. 2: Detailed model of inverter system.

the measured amplitude V_M. The transient model given in Appendix B is

$$\begin{bmatrix}\delta V_M \\ \delta f_M\end{bmatrix} = T_{\text{pll}} \begin{bmatrix}\Re\delta V_N \\ \Im\delta V_N\end{bmatrix}, \tag{15}$$

$$\begin{bmatrix}\Re\delta V_N' \\ \Im\delta V_N'\end{bmatrix} = T_{\text{arg}} \begin{bmatrix}\Re\delta V_N \\ \Im\delta V_N\end{bmatrix}. \tag{16}$$

E. PI Controller

The discrepancies between the measurements f_M, V_M and the desired values f_D, V_D are fed into two PI controllers for the longitudinal, r, and radial, θ, control signals. Appendix B gives the model of the form

$$\begin{bmatrix}\delta r \\ \delta\theta\end{bmatrix} = T_{\text{PI}} \left(\begin{bmatrix}\delta V_D \\ \delta f_D\end{bmatrix} - \begin{bmatrix}\delta V_M \\ \delta f_M\end{bmatrix} \right) \tag{17}$$

In the numerical examples, we assume zero P gain of the controllers, which are therefore I controllers.

F. Phase Converter

The phase converter transforms the control signals r and θ (see Appendix B-D) to phasor V_P (in Cartesian coordinates). Input V_N' from the PLL is used to align V_P with the instantaneous phase of the voltage V_N. Appendix B has

$$\begin{bmatrix}\Re\delta V_P \\ \Im\delta V_P\end{bmatrix} = T_{\text{ph1}} \begin{bmatrix}\Re\delta V_N' \\ \Im\delta V_N'\end{bmatrix} + T_{\text{ph2}} \begin{bmatrix}\delta r \\ \delta\theta\end{bmatrix}, \tag{18}$$

where $\delta\theta$ and δr come from in (17).

G. Inverter Gain

Appendix B discusses the constant gain model

$$\delta V_C = K_{\text{inv}} \delta V_P, \tag{19}$$

where δV_P is the phasor from (18).

H. Inverter Circuit and Grid Circuit

The inverter circuit has two voltage sources V_C and V_G. As an additional input, the load impedance Z_L is used to model load power changes. Appendix B derives the model as

$$\begin{bmatrix}\delta\Re V_N \\ \delta\Im V_N \\ \delta\Re I_N \\ \delta\Im I_N\end{bmatrix} = T_{\text{ckt1}} \begin{bmatrix}\delta\Re V_C \\ \delta\Im V_C\end{bmatrix} + T_{\text{ckt2}} \begin{bmatrix}\delta\Re V_G \\ \delta\Im V_G\end{bmatrix} + T_{\text{ckt3}} \begin{bmatrix}\delta\Re Z_L \\ \delta\Im Z_L\end{bmatrix}. \tag{20}$$

I. Exogenous Disturbances

This paper considers three examples of disturbances: load power disturbance, power set-point disturbance, and grid frequency disturbance. Inverter load power disturbance $(\delta P_L, \delta Q_L)$ is modeled through a change in the load impedance δZ_L, which is coupled to the system through (20). The model of the power set-point disturbance is given by (14).

Appendix B models grid frequency disturbance through phasor V_G as

$$\delta V_G = |V_G| e^{i\phi_G} i\delta\phi_G = V_G i\delta\phi_G. \tag{21}$$

This and the transient counterpart of (1) yields the disturbance input phasor δV_G

$$\begin{bmatrix}\Re\delta V_G \\ \Im\delta V_G\end{bmatrix} = \frac{2\pi}{s} \begin{bmatrix}-\Im V_G \\ \Re V_G\end{bmatrix} \delta f_G = T_{\text{frq}}\, \delta f_G.$$

J. Closed-loop Transfer Function

Subsections Appendix B-B through Appendix B-G describe perturbation transfer function of each block in Figure 2. By connecting these transfer functions, we can form a closed-loop transfer function. We can also include the disturbances according to Section III-I.

The left side of the system diagram in Figure 2 is a physical circuit, whereas the right side is the control logic. The control signal V_C and the measurements (V_N, I_N) connect the two sides. The transient model of circuit in the left side has δV_C as input and $(\delta V_N, \delta I_N)$ as output. Furthermore, it has δV_G as a grid frequency disturbance input and δZ_L as a load power disturbance input. The overall circuit model has the form

$$\begin{bmatrix}\Re\delta V_N \\ \Im\delta V_N \\ \Re\delta I_N \\ \Im\delta I_N\end{bmatrix} = G_{\text{ckt}} \begin{bmatrix}\Re\delta V_C \\ \Im\delta V_C\end{bmatrix} + H_{\text{ckt}} \begin{bmatrix}\Re\delta V_G \\ \Im\delta V_G \\ \delta\Re Z_L \\ \delta\Im Z_L\end{bmatrix} \tag{22}$$

Similarly, the model of the control logic on the right side has $(\delta V_N, \delta I_N)$ as input and δV_C as output. It also has $(\delta P_{set}, \delta Q_{set})$ as power set-point disturbance input.

$$\begin{bmatrix}\Re\delta V_C \\ \Im\delta V_C\end{bmatrix} = G_{\text{logic}} \begin{bmatrix}\Re\delta V_N \\ \Im\delta V_N \\ \Re\delta I_N \\ \Im\delta I_N\end{bmatrix} + H_{\text{logic}} \begin{bmatrix}\delta P_{set} \\ \delta Q_{set}\end{bmatrix}. \tag{23}$$

Equations (22) and (23) describe the closed-loop transfer function model of a single inverter transfer function matrices

$$\frac{\delta f_N(s)}{\delta f_G(s)} = T_{f_N}\left(I - T_{\text{ckt1}}K_{\text{inv}}\left(T_{\text{ph2}}T_{\text{PI}}\left(T_{\text{droop}}T_{\text{msr}} - \begin{bmatrix}T_{\text{pll}} & 0\end{bmatrix}\right) + T_{\text{ph1}}\begin{bmatrix}T_{\text{ag}} & 0\end{bmatrix}\right)\right)^{-1} T_{\text{ckt2}}T_{\text{frq}} \tag{24}$$

in accordance with (13), (14), (15), (16), (17), (18), (19), and (20), where δP_{set}, δQ_{set}, δV_G, and δZ_L are exogenous inputs,

$$\begin{aligned} G_{\text{logic}} &= K_{\text{inv}}\left(T_{\text{ph2}}T_{\text{PI}}\left(T_{\text{droop}}T_{\text{msr}} - \begin{bmatrix}T_{\text{pll}} & 0\end{bmatrix}\right)\right. \\ &\qquad \left. + T_{\text{ph1}}\begin{bmatrix}T_{\text{ag}} & 0\end{bmatrix}\right), \\ H_{\text{logic}} &= K_{\text{inv}}T_{\text{ph12}}T_{\text{PI}}T_{\text{droop}}, \\ G_{\text{ckt}} &= T_{\text{ckt1}}, \\ H_{\text{ckt}} &= \begin{bmatrix}T_{\text{ckt2}} & T_{\text{ckt3}}\end{bmatrix}. \end{aligned}$$

The closed-loop transfer function for the grid frequency disturbance follows from (22) and (23) with $\delta Z_L = 0$ and $\delta P_{set} = 0$, and $\delta Q_{set} = 0$. This yields (24), see the page top. We take $\delta f_N = T_{f_N}\delta V_N$, where T_{f_N} is derived similar to (21). One can similarly derive the closed-loop transfer functions for power set-point disturbances and load power disturbances.

IV. Multiple Inverters

A model of a distribution system with multiple inverters is illustrated in Figure 3. This model is an extension of that of Figure 1. The feeder is shown as the voltage source V_G with infinite capacity. The shaded box showing the distribution circuit combines medium voltage (MV) and LV power distribution circuits. The distribution circuit is connected to m customers, each is modeled by an aggregated load and an inverter-connected distributed generation (DG) resource. The analysis in this section is applicable to distribution circuits with any topology.

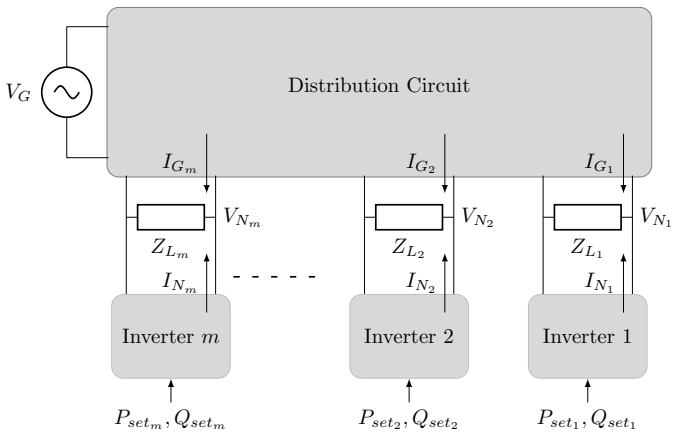

Fig. 3: Multiple inverter circuits.

A. Notations

In our model, the distribution system serves m customers. Customer k is modeled by an aggregated load shown as an impedance $Z_{L_k} \in \mathbb{C}$. Customer k is modeled by an ideal controlled voltage source V_{C_k} and an inverter circuit. The voltage V_{C_k} is dependent on the control logic, the power set-points P_{set_k}, Q_{set_k}, and the measurements V_{N_k} and I_{N_k}, as shown in the inverter block in Figure 2. Inverter k generates output active and reactive power P_{N_k} and Q_{N_k}. Customer k draws current I_{G_k} from the distribution circuit.

We use notation similar to the single inverter problem and add subscripts k for the customers $k = 1, 2, \ldots, m$. Denote $\bar{V}_C = \begin{bmatrix}V_{C_1} & V_{C_2} & \ldots & V_{C_m}\end{bmatrix}^T$. We use similar notations for $\delta\bar{V}_C$. We denote

$$\overline{\begin{bmatrix}V_N \\ I_N\end{bmatrix}} = \begin{bmatrix}V_{N_1} & I_{N_1} & V_{N_2} & I_{N_2} & \ldots & V_{N_m} & I_{N_m}\end{bmatrix}^T,$$

and use similar notations for $\overline{\begin{bmatrix}V_N \\ I_G\end{bmatrix}}$, and $\overline{\begin{bmatrix}\delta V_N \\ \delta I_N\end{bmatrix}}$.

The inverter system model in this section is the same as that shown in Figure 2 and described in Section III, except that the variables now carry the index k corresponding to the customer/inverter.

B. Linear Circuit Model

In what follows, we develop a systematic approach to determine the transfer function $\bar{G}_{\text{ckt}}$ that is analogous to G_{ckt} in (22). The distribution circuit, which is assumed to be linear, can be represented by

$$\bar{I}_G = X\bar{V}_N + YV_G \tag{25}$$

for some (complex) matrices $X \in \mathbb{C}^{m\times m}$ and $Y \in \mathbb{C}^{m\times 1}$.

The inverter circuit model generalizes single inverter expression (58). For multiple inverters, the open-loop relation between V_C and V_N and I_N becomes

$$V_{C_k} = T_{\text{inv},k}\begin{bmatrix}V_{N_k} \\ I_{N_k}\end{bmatrix}, \tag{26}$$

where $T_{\text{inv},k}$ is derived from applying KVL, KCL, and Ohm's law to the inverter circuit. From (26), we get

$$\bar{V}_C = W\overline{\begin{bmatrix}V_N \\ I_N\end{bmatrix}} = WP\begin{bmatrix}\bar{V}_N \\ \bar{I}_N\end{bmatrix}, \tag{27}$$

where P is a permutation matrix such that $\overline{\begin{bmatrix}V_N \\ I_N\end{bmatrix}} = P\begin{bmatrix}\bar{V}_N \\ \bar{I}_N\end{bmatrix}$ and W is the diagonal matrix

$$W = \begin{bmatrix}T_{\text{inv},1} & & \\ & \ddots & \\ & & T_{\text{inv},m}\end{bmatrix}.$$

At each load, we have two port network

$$\begin{bmatrix}V_{N_k} \\ I_{G_k}\end{bmatrix} = T_{\text{load},k}\begin{bmatrix}V_{N_k} \\ I_{N_k}\end{bmatrix}, \tag{28}$$

We aggregate the load transfer function as

$$M = \begin{bmatrix}T_{\text{load},1} & & \\ & \ddots & \\ & & T_{\text{load},m}\end{bmatrix}$$

We then have $\overline{\begin{bmatrix} V_N \\ I_G \end{bmatrix}} = M \overline{\begin{bmatrix} V_N \\ I_N \end{bmatrix}}$, and $\begin{bmatrix} \bar{V}_N \\ \bar{I}_G \end{bmatrix} = P^{-1} M P \begin{bmatrix} \bar{V}_N \\ \bar{I}_N \end{bmatrix}$. By substituting this into (27) and solving for $\bar{V}_N$, we get

$$\bar{V}_N = \left(W M^{-1} P \begin{bmatrix} I \\ X \end{bmatrix} \right)^{-1} \left(\bar{V}_C - W M^{-1} P \begin{bmatrix} 0 \\ Y \end{bmatrix} V_G \right). \tag{29}$$

Substituting (29) into (27) we can solve for $\bar{I}_N$.

C. Closed-loop Transfer Function

Our analysis approach requires finding the steady-state solution first. Similar to the single inverter problem, the circuits and most of the control logic are linear, however, the power measurement and coordinate transforms are nonlinear. Finding the steady-state requires solution of nonlinear equations. For some specific topologies, a closed-form steady-state solution can be found, for example, see Appendix A. In a general case, the solution has to be computed numerically. In what follows we assume that such a solution is available.

The control logic for each of the inverters is described in Section III and summarized by the transfer functions G_{logic} and H_{logic} (23). In this section, each of the m inverters is described by the transfer functions of the same form

$$\delta V_{C_k} = G_{\text{logic},k} \begin{bmatrix} \delta V_{N_k} \\ \delta I_{N_k} \end{bmatrix} + H_{\text{logic},k} \begin{bmatrix} \delta P_{set,k} \\ \delta Q_{set,k} \end{bmatrix} \tag{30}$$

The distribution circuit, all inverter circuits, and all loads are linear circuits. The only voltage sources in Figure 3 model are $V_{C_1}, \ldots, V_{C_m}$ and V_G. Thus, we can find the linear map from $V_{C_1}, \ldots, V_{C_m}$ and V_G to $V_{N_1}, \ldots, V_{N_m}$ and $I_{N_1}, \ldots, I_{N_m}$ as described in Section IV-B. For the linearized model, we get

$$\overline{\begin{bmatrix} \delta V_N \\ \delta I_N \end{bmatrix}} = \bar{G}_{\text{ckt}} \delta \bar{V}_C + \bar{H}_{\text{ckt}} \begin{bmatrix} \delta V_G \\ \delta \bar{Z}_L \end{bmatrix}. \tag{31}$$

This is multiple-inverter version of (22) and (23). Combining (30) and (31), we can form a closed-loop transfer function. The exogenous disturbances of the closed-loop system include $\delta P_{set,k}$, $\delta Q_{set,k}$ for the power set-point disturbances, δZ_{L_k} for the load power disturbances, and δV_G for grid frequency disturbances, as described in Section III-I. This completes the analysis for the distribution system with multiple inverters.

V. Single Inverter Analysis

To illustrate the engineering use of the proposed analysis approach, this and the next section consider two examples. This section considers the first example, a lumped single inverter model introduced in Subsection V-A. It is analyzed for grid frequency rejection performance in Subsection V-B and verified against a detailed simulation in Subsection V-C.

A. Single Inverter Model

This example considers a lumped single inverter model in a distribution system. The model aggregates multiple inverter-connected DG resources and follows a related example in [18]. Figure 4 shows a feeder that serves a distribution system with 150 customers, each has a constant 2kVA load. The power is delivered through a long distance MV grid (2.4kV

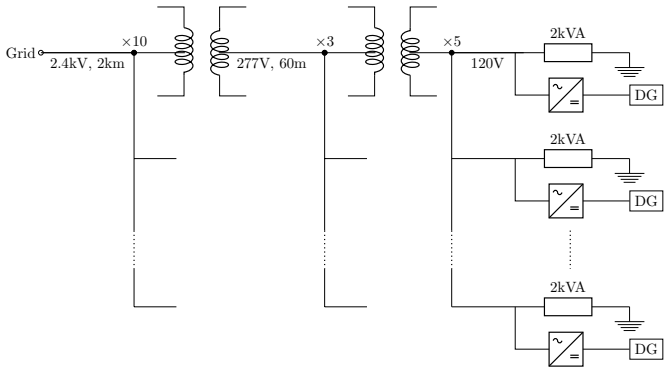

Fig. 4: Distribution system schematics before aggregation.

carried by a 2km line with American wire gauge (AWG)$3/0$) and shorter distance LV grid (277V, AWG$1/0$, 60m). The power is delivered from the pole to the customers with LV (120V, AWG3) with line distance ranging from 10m to 100m. We consider only the LV/MV line impedance here, since the equivalent impedance of the HV lines beyond feeder are comparatively small in the LV equivalent model.

The lumped model aggregates the multiple inverter system into a single inverter model by assuming that all voltage branches have the same voltage. The line impedances of the corresponding branches are then connected in parallel. The combined circuit nodes are marked as $\times 3$, $\times 5$, and $\times 10$ in Figure 4, specifying the respective numbers of aggregated branches. This lumped model is not exact, yet it is a good approximation for initial analysis.

We use the term *installation rate* to mean the ratio of customers with inverter-connected DG to the total customer number. We will also introduce the term *utilization rate* as the ratio of the DG output power to the DG power rating, for example, due to insolation.

The lumped model parameters can be derived from parameters of the individual branches before the aggregation. The lumped impedance of the 277V line is 10 times smaller. For the 120V line, it is $150 = 10 \times 3 \times 5$ smaller. Let the installation rate be r_{ins} and the total number of inverters m. Compared to an individual inverter, the lumped power is mr_{ins} times larger. In accordance with Subsection II-D, the lumped model droop gains are mr_{ins} times smaller than that for an individual inverter. Other lumped inverter parameters, such as the PI controller gains, are the same as for an individual inverter. The utilization rate r_{utz} affects the individual DG output power according to $P_{N,\text{max}} = r_{\text{utz}} P_{\text{rating}}$, where P_{rating} is power rating of DG. We take $P_{\text{rating}} = 2\text{kW}$ here.

B. Single Inverter Disturbance Rejection Analysis

Consider grid frequency disturbance amplification in the distribution system of Section V-A. As a performance metric, we compute the H_∞ norm of the transfer function from the grid frequency variation δf_G to the inverter frequency variation δf_N. The H_∞ norm measures the worst case amplification over all frequencies of the input disturbance.

Copies of the same inverter might work in different distribution systems. From this perspective, it is of interest if there

TABLE I: Parameter sweep.

Parameters	Minimum Value	Maximum Value
Installation Rate	0.23	0.95
Utilization Rate	0.23	0.95
Power Factor	0.9	1.00
Line Distance	20m	100m

is a set of inverter tuning parameters that works for a variety of distribution systems scenarios and operating conditions.

We considered the following fixed inverter parameters. For the PLL model (53), we took $\zeta_p = 0.65$ and $w_p = 57$. For the LCL filter, we used $R_f = 2\Omega$, $L_f = 1 \cdot 10^{-3}$H, and $C_f = 500\mu$F. The LCL filter resonance frequency was $L_f C_f = 5 \cdot 10^{-7}$, as in [19]. The bandpass filter in (48) takes $K_b = 1500$. The transformer model described in Appendix B-G has $R_1 = 0.026\Omega$, $R_2 = 8.7 \cdot 10^{-3}\Omega$, $L_1 = 2.75 \cdot 10^{-3}$H, $L_2 = 9.2 \cdot 10^{-4}$H, $R_m = 25958\Omega$, and $L_m = 68.857$H.

The PI controller gains were designed to provide (i) step responses for the power set-point that settle in less than 0.5 sec for medium line distance (100 m) and medium inverter output power (several kW) and (ii) stability for all parameters in Table I. For each point on a coarse grid of K_{θ_I} and K_{r_I}, we simulated the middle and the eight corner cases for Table I. The gains $K_{\theta_I} = 0.132$ and $K_{r_I} = 18.85$ were selected.

The opposite droop controller gain was determined as described in Subsection II-D. To comply with IEEE 1547, we must have $f_N \in [59.8, 60.5]$ and $|V_N| \in [120 \cdot 88\%, 120 \cdot 110\%]$. These requirements define $f_{N,\max}$, $f_{N,\min}$, $|V_N|_{\max}$, and $|V_N|_{\min}$ when setting the droop gains in accordance with Subsection II-D. IEEE 1547 required the power factor to be least 85%. We take

$$P_{set} = P_{N,\max} \cdot \frac{12}{12 + 14.4}, \quad P_{N,\min} = 0 \quad (32)$$

$$Q_{N,\max} = P_{N,\max} \cdot \tan(\cos^{-1} 0.85), \; Q_{N,\min} = -Q_{N,\max} \quad (33)$$

We studied variations of inverter operating conditions in a distribution system as described by four parameters in the lumped model of Subsection V-A. These parameters are installation rate, utilization rate, load power factor, and distribution line distance. Their ranges are shown in Table I. To analyze the inverter performance, the range of each parameter is sampled at 5 points. The sweep over the grid of the parameter values considers the total of $5^4 = 625$ parameter combinations.

Using line impedance data for from [20] and [18], we compute the line impedances as $0.2627 + i0.1378\Omega$/km for the AWG $3/0$ lines, $0.3863 + i0.0944\Omega$/km for the AWG $1/0$ lines, and $0.7972 + i0.1056\Omega$/km for the AWG 3 lines. The line impedance is linear in distance, for example, the LV (120V, AWG3) grid impedance $Z_{LV} = (0.7972 + i0.1056) \cdot (D/1000)$ where D is the LV line distance in meters.

The results of the parameter sweep are shown in Figure 5. The subplots in Figure 5 show the projections of the 625 computed H_∞ norms on the four parameter axes. For each sample value of the parameter, the markers show the the H_∞ norms for all analyzed combinations of other parameters.

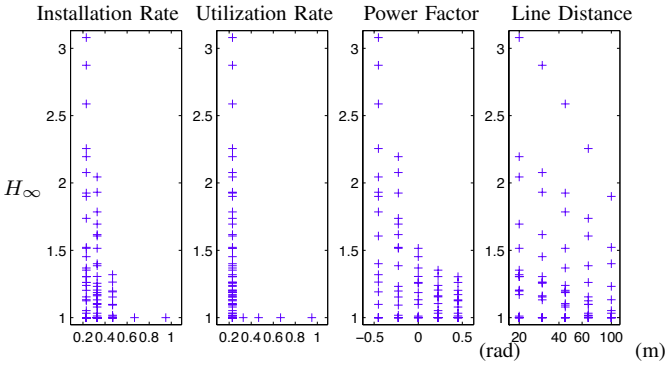

Fig. 5: Transient analysis of the grid frequency disturbances.

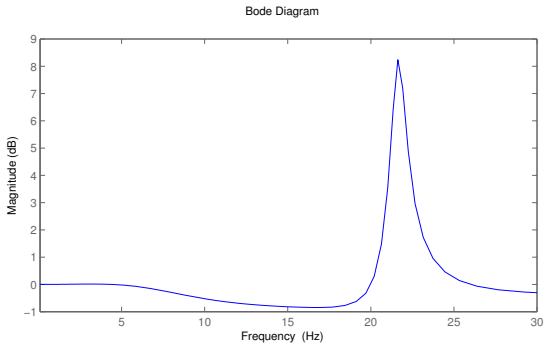

Fig. 6: Magnitude Bode plot with high H_∞ norm.

The results demonstrate that the H_∞ norm is less than 2.5 for most sample points considered. However, when the installation rate and utilization rate are both small, the load is capacitive (the negative power factor), and the distribution line is short, the H_∞ norm can be high, indicating oscillatory behavior at the resonance frequency, see Figure 6. When utilization rate is smaller than 0.2 (outside of the displayed range) the system might even go unstable. The instability is caused by large droop gains caused by the design described in Subsection II-D. In accordance with (32) and (33), the droop gains can be arbitrary large for a small utilization rate P_{set} because the denominators in the droop gain expression are small. This problem can be avoided by limiting the droop gains. Note that even when the droop gains are large, the H_∞ norm is relatively small for a longer distribution line, as shown in Figure 5. In fact, large line impedance is assumed in [5], [7] so the described problem was not noticed there.

C. Single Inverter Detailed Simulation

The analysis model described in Section III and Subsections V-A and V-B was verified against a very detailed 3-phase simulation of the distribution system with a single droop inverter. The simulation was developed in MATLAB/Simulink using the SimPowerSystems toolbox and its component model templates for electric power generation, transmission, distribution, and control [21].

The detailed inverter model in Simulink was based on a modified three bridge 3-phase DC-AC gridtie inverter model in SimPowerSystems [21]. The inverter control logic provide detailed implementation of these in Figure 2. The grid

frequency, phase, and amplitude measurement are obtained using the PLL logic block from the SimPowerSystems. The instantaneous values of P_N and Q_N are measured through a SimPowerSystems discrete power measurement block every millisecond. The PLL and power measurements go through a band-pass filter with a 30Hz-wide band centered at 60Hz.

The droop controller is implemented as an algebraic expression, and the PI controllers are implemented using Simulink discrete integral controller blocks. The phase converter block, which generates a 3-phase signal that controls the switching pulses for the IGBT gates of the inverter, is implemented through the $dq0 \mapsto abc$ and polar-to-Cartesian transformation blocks from the SimPowerSystems. The simulation included pulse-width modulated voltage that goes through an LCL filter to remove higher order harmonics. The LCL filter includes an RC snubber circuit to dampen out the transients.

The utility grid, as seen from the distribution grid, is simulated as a constant voltage source that may have varying frequency. This is built into the model by using the Three-Phase Programmable Voltage Source from the SimPowerSystems toolbox that allows for step and ramp changes in frequency and phase. The utility grid voltage source is connected to the load through a realistic 3-phase distribution line model. SimPowerSystems contains models of loads where active power (P_N) and reactive power (Q_N) can be explicitly specified. This load is then connected to ground.

The detailed simulations were used to verify the transfer functions in the small-signal analysis model of this paper. The two models yield very close results. This can be seen from the differences in their responses to unit steps plotted in Figure 7.

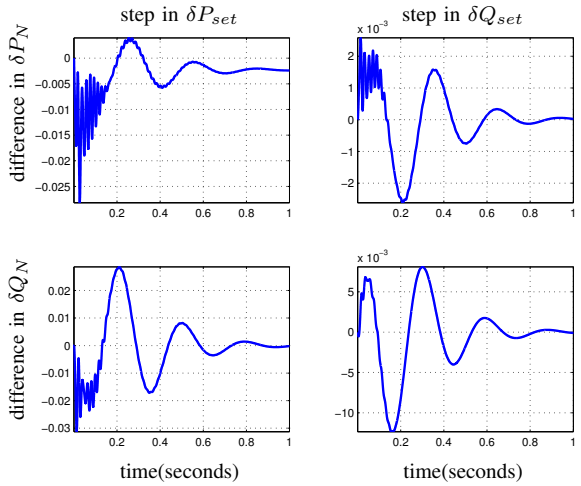

Fig. 7: Difference of the Power Set-point Disturbance Step Between Detailed Simulation and Analysis Model

For a selected set of the parameters in Table I, computing the transfer functions and the H_∞ norm takes approximately 1 second. This is much faster than the total run time of around 10 minutes when computing disturbance amplification for given model parameters using the detailed simulation model.

VI. Multiple Inverter Analysis

This section considers the second example, a multiple inverter system. The model is introduces in Section VI-A. It is used in Section VI-B to analyze voltage power setpoint disturbance and in Section VI-C for controller tuning. We considers the opposite droop inverter in this section.

A. Multiple Inverter Model

We demonstrate analysis for a distribution system with many inverters, that is beyond the reach of most existing detailed simulation packages. We consider a distribution system with 40 customers, connected in a linear topology.

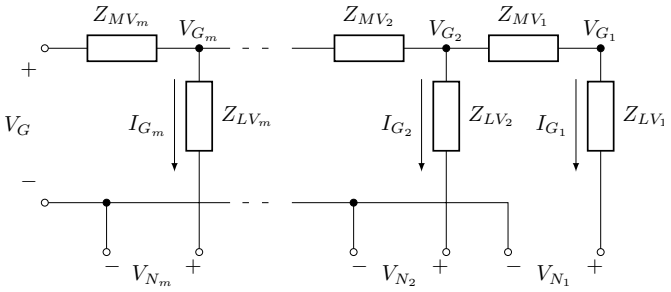

Fig. 8: Distribution circuit.

The distribution circuit is illustrated in Figure 8. The impedances Z_{MV_k} model the overhead power line and include the equivalent MV grid impedance as seen from the LV grid. The connection impedances Z_{LV_k}, model the lines connecting the houses to the pole-mounted transformers. For simplicity, all inverters are assumed identical, apart from their operating set-points. The model of each inverter and the line impedance models are the same as described in Section V-B.

We assume 20m long LV line and 7km long MV line with evenly spaced LV/MV transformers. All loads are identical, each has rating 10kVA and power factor 0.98. The installation rate is 100%, and each opposite droop inverter has power set-point of 4kW.

The methodology of Section IV requires to build a linear map (25) for the distribution circuit in Figure 8. A model of the distribution circuit can be written as

$$\begin{aligned}\left(V_{N_{k+1}} + Z_{LV_{k+1}} I_{G_{k+1}}\right) - \left(V_{N_k} + Z_{LV_k} I_{G_k}\right) \\ = Z_{MV_k} \sum_{j=1}^{k} I_{G_j},\end{aligned} \tag{34}$$

for $k = 1, 2, \ldots, m-1$, with the boundary condition

$$V_G - \left(V_{N_m} + I_{G_m} Z_{LV_m}\right) = Z_{MV_m} \sum_{j=1}^{m} I_{G_j}. \tag{35}$$

Equations (34) and (35) correspond to (25) with $X = -\bar{R}^{-1} L^{-T}$ and $Y = \bar{R}^{-1} e_m$, with

$$\bar{R} = \operatorname{diag}(\bar{Z}_{MV}) L + (I - D^T) \operatorname{diag}(\bar{Z}_{LV}), \tag{36}$$

where I is the identity matrix, D is the unit shift matrix (1 in the subdiagonal entries and 0 elsewhere), e_m is the m-th unit vector, and L is a lower triangular matrix of ones. Note that $L^{-1} = I - D$. With X and Y given, the circuit equations in Section IV follow.

B. Multiple Inverter Power Disturbance Response

The formulated model allows evaluation of how disturbances affect line voltage profile. Figure 9 shows a scenario where a cloud drifts through the area of the distribution system with linear topology. Suppose the 20 inverters furthest from the feeder suddenly reduce their power output as the solar panels are shaded. The voltage profile impact can be modeled by applying an appropriate power set-point inputs to the power $\rightarrow$ voltage transfer function derived in Section VI-A.

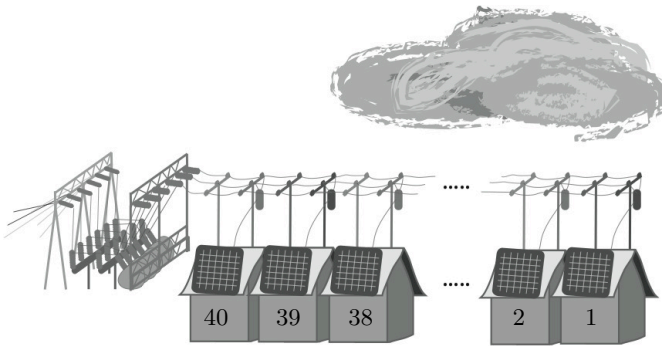

Fig. 9: Multiple inverters. Power set-point disturbance.

Figure 10 shows the voltage profile deviation over time when $\{\delta P_{set,k}\}_{k=0,\ldots,20}$ all decrease by 4kW at $t = 0$. We change the sign of the z-axis for illustration. For customers 1 to 20, P_N and V_N change in accordance with (12). The net loads for these customers start drawing current from the grid, resulting a significant voltage drop for $V_{G,0}$ through $V_{G,20}$. A 0.42V transient peak appears in $\delta V_{G,1}$ in the first 0.4s, in addition to the 1.79V steady-state change.

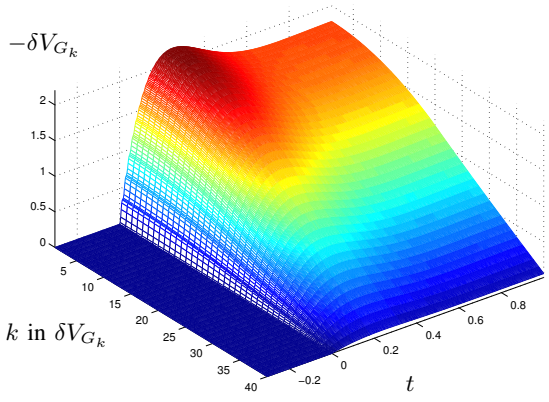

Fig. 10: Voltage profile. Power set-point disturbance.

The described methodology allows evaluation of the voltage profile deviations and voltage transients for other more complicated scenarios. This could help to evaluate the compliance with IEEE 1547 for high penetration of DG.

C. Controller Gain Tuning

The multiple-inverter model of Section VI-A can be used to generate design information for inverter controller. Specifically, we are interested in controller tuning that ensures closed loop performance for varying problem parameters. We assume that the distribution system model in Figure 8 has $m = 5$ inverters. The rest of the system parameter, unless specially noted below, take the same values as in Section VI-A.

We vary two key problem parameters, controller gain and line distance. The varying gain relates to the PI Controller in Figure 8. The droop controller gain is specified as described in Section II-D and is defined by the power setpoint. The PI Controller (17) is assumed to have I-gains for the magnitude channel, $K_{\theta_I} = 0.132 \cdot c$, and for the phase channel, $K_{r_I} = 18.85 \cdot c$, where c is a (positive) gain parameter we wish to vary and tune. The line distance D is assumed to be the same for each inverter. The distances D define load impedances $Z_{LV,k}$, shown Figure 8, as described in Section V-B.

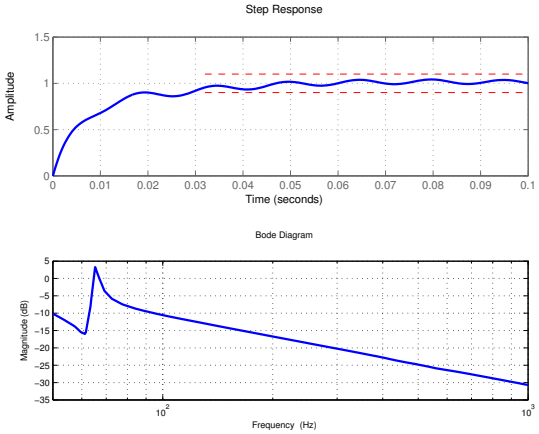

Fig. 11: Step response (top) and Bode plot (bottom) for gain $c = 2.67$ and line distance $D = 105$m.

For given problem parameters, closed loop performance is described by two parameters illustrated in Figure 11. First, the disturbance rejection is described by $H_\infty(T_f)$ where T_f is transfer function from the grid frequency variation δf_G to the vector of the inverter frequency variations $\delta \bar{f}_N$. The H_∞ norm is the peak of the magnitude Bode plot, the lower subplot in Figure 11. Large H_∞ norm means the system amplifies grid frequency variation. It implies the poles are close to the stability boundary. Second, the closed-loop step response, the upper subplot in Figure 11, is described by the rise time, the time it takes to get into $\pm 10\%$ bounds of the step.

Figure 12 summarizes the controller design information in the space of the problem parameters c and D. For larger controller gain c, the rise time is smaller. At the same time, the H_∞ norm increases and the response becomes very oscillatory. When frequency disturbance are amplified by more than 80%, the H_∞ norm increases with the gain c quickly and then the system becomes unstable. We consider such large H_∞ norm or unstable system unacceptable. This is indicated by empty bars in Figure 12. For the considered range of the line distances in Figure 12, the gains between $c = 1.94$ and $c = 2.75$ appear to give the best design: the rise time is small while disturbance amplification and stability characterized by H_∞ norm are acceptable.

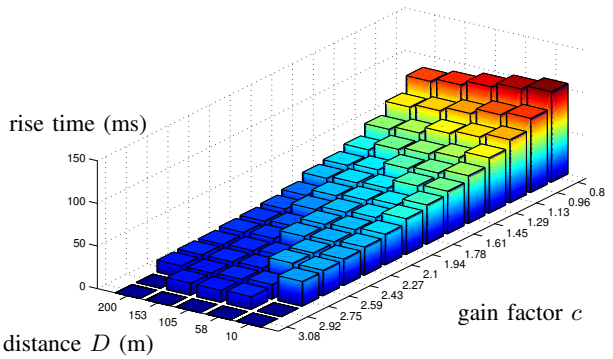

Fig. 12: Rise time dependence on gain and line distance.

VII. Conclusion

This paper develops a methodology for analysis of inverter-connected distributed generations using linearized models. It addresses the gap between the well established methodology for analysis of bulk generation and transmission systems and much less developed analysis of inverter-connected distributed generation. The formulated analysis approach takes into account the closed-loop system dynamics introduced by multiple inverters and is applicable to different types of inverters and distribution topologies. The examples show applicability to frequency stability analysis, gain tuning for inverter controllers, and analysis of voltage profile response to distributed power generation disturbances.

References

[1] H. Saadat, *Power System Analysis*. PSA Publishing, 2010.

[2] J. A. P. Lopes, C. L. Moreira, and A. G. Madureira, "Defining control strategies for microgrids islanded operation," *IEEE Trans. on Power Systems*, vol. 21, no. 2, pp. 916–924, 2006.

[3] C. K. Sao and P. W. Lehn, "Autonomous load sharing of voltage source converters," *IEEE Trans. on Power Delivery*, vol. 20, no. 2, pp. 1009–1016, 2005.

[4] W. Yao, M. Chen, J. Matas, J. M. Guerrero, and Z.-M. Qian, "Design and analysis of the droop control method for parallel inverters considering the impact of the complex impedance on the power sharing," *IEEE Trans. on Industrial Electronics*, vol. 58, no. 2, pp. 576–588, 2011.

[5] H. J. Avelar, W. A. Parreira, J. B. Vieira Jr., L. C. G. de Freitas, and E. A. A. Coelho, "A state equation model of a single-phase grid-connected inverter using a droop control scheme with extra phase shift control action," *IEEE Trans. on Industrial Electronics*, vol. 59, no. 3, pp. 1527–1537, 2012.

[6] J. M. Guerrero, L. G. de Vicuna, J. Matas, M. Castilla, and J. Miret, "A wireless controller to enhance dynamic performance of parallel inverters in distributed generation systems," *IEEE Trans. on Power Electronics*, vol. 19, no. 5, pp. 1205–1213, 2004.

[7] E. A. A. Coelho, P. C. Cortizo, and P. F. D. Garcia, "Small-signal stability for parallel-connected inverters in stand-alone ac supply systems," *IEEE Trans. on Industry Applications*, vol. 38, no. 2, pp. 533–542, 2002.

[8] A. Engler, "Applicability of droops in low voltage grids," *Internat. J. of Distributed Energy Resources*, vol. 1, no. 1, pp. 3–15, 2005.

[9] N. Pogaku, M. Prodanovic, and T. Green, "Modeling, analysis and testing of autonomous operation of an inverter-based microgrid," *IEEE Trans. on Power Electronics*, vol. 22, no. 2, pp. 613–625, 2007.

[10] S. V. Iyer, M. N. Belur, and M. C. Chandorkar, "A generalized computational method to determine stability of a multi-inverter microgrid," *IEEE Trans. on Power Electronics*, vol. 25, no. 9, pp. 2420 – 2432, 2010.

[11] C.-T. Lee, C.-C. Chu, and P.-T. Cheng, "A new droop control method for the autonomous operation of distributed energy resource interface converters," *IEEE Trans. on Power Electronics*, vol. 28, no. 4, pp. 1980 – 1993, 2013.

[12] R. Majumder, B. Chaudhuri, A. Ghosh, R. Majumder, G. Ledwich, and F. Zare, "Improvement of stability and load sharing in an autonomous microgrid using supplementary droop control loop," *IEEE Trans. on Power Systems*, vol. 25, no. 2, pp. 796 – 808, 2010.

[13] G. Díaz, C. González-Morán, J. Gómez-Aleixandre, and A. Diez, "Scheduling of droop coefficients for frequency and voltage regulation in isolated microgrids," *IEEE Trans. on Power Systems*, vol. 25, no. 1, pp. 489–496, 2010.

[14] H. Liang, B. J. Choi, W. Zhuang, and X. Shen, "Stability enhancement of decentralized inverter control through wireless communications in microgrids," *IEEE Trans. on Smart Grid*, vol. 4, pp. 321–331, 2013.

[15] E. Glover, C.-C. Chang, D. Gorinevsky, and S. Lall, "Frequency stability for distributed generation connected through grid-tie inverter," in *IEEE Conference on Power Systems Technology*, 2012.

[16] EPRI, "Integrating smart distributed energy resources with distribution management systems," Tech. Rep. 1024360, 2012.

[17] K. D. Brabandere, "Voltage and frequency droop control in low voltage grids by distributed generators with inverter front-end," Ph.D. dissertation, University of Leuven, Leuven, Belgium, 2006.

[18] R. H. Lasseter and P. Piagi, "Control and design of microgrid components," in *Final Project Report – PSERC Publication 06-03*, 2006.

[19] P. Channegowda and V. John, "Filter optimization for grid interactive voltage source inverters," *IEEE Trans. on Industrial Electronics*, vol. 57, no. 12, pp. 4106–4114, 2010.

[20] G. E. Company, *Distribution Data Book: A Collection of Fundamental Data Pertaining to the Elements Of, and the Loads On, Distribution Systems*. General Electric, 1972.

[21] Mathworks. (2011) Recorded webinar: Modeling and simulation of PV solar power inverters. [Online]. Available: http://www.mathworks.com/wbnr57525

[22] T. C. Wang, S. Lall, and T. Y. Chiou., "Polynomial method for PLL controller optimization," *Sensors*, vol. 11, no. 7, pp. 6575–6592, 2011.

Appendix A
Steady-state Solution

To find the steady-state of the distribution circuit model in Figure 2, we assume that the following parameters are given:

- distributed generation penetration: $a = P_N/P_L$, (the fraction of the active power produced by inverters)
- power factor of the load: $\cos(\psi)$ with $\psi = \angle(P_L + iQ_L)$,
- magnitude of the load power: $|P_L + iQ_L|$,
- transmission line impedance: $Z_G = |Z_G|\angle\gamma$,
- utility grid voltage: $V_G = 120V\angle 0$,
- inverter parameters: K_f and K_V
- inverter power set-points: P_{set} and $Q_{set} = 0$

In the steady-state,

$$f_N = f_D, \quad |V_N| = V_D, \tag{37}$$

and P_N and Q_N follow the droop equations. The steady-state for variables inside an inverter can then be calculated from circuit equations and control logics. The steady-state solves (3), (4), (5), (6), (8), (10), and (37). There are 14 (real) equations and 14 unknowns: P_N, Q_N, P_G, Q_G, $|V_N|$, ϕ_N, $|I_N|$, $\angle I_N$, I_G, $\angle I_G$, f_D, V_D, $\Re Z_L$, $\Im Z_L$.

In accordance with (10), (37), and the made assumptions

$$P_N = P_{set}, \tag{38}$$

$$|V_N| = V_{N,0} - K_V Q_N, \tag{39}$$

Let $I_N = |I_N|\angle(\phi_N + \varphi)$ and $I_G = |I_G|\angle(\phi_N + \theta)$. After we express I_G in (6) from (3), (5) and (6) become

$$P_N + iQ_N = |V_N||I_N|\angle -\varphi, \tag{40}$$

$$P_G + iQ_G = \frac{|V_N||V_G|\angle\phi_N}{|Z_G|\angle -\gamma} - \frac{|V_N|^2}{|Z_G|\angle -\gamma}, \tag{41}$$

According to (38) and (39), (8) becomes

$$P_G + iQ_G = (P_L + iQ_L) - \left(P_{set} + i\frac{V_{N,0} - |V_N|}{K_V}\right). \tag{42}$$

This, along with (41), yields two (real) equations

$$\frac{|V_N||V_G|}{|Z_G|}\cos(\phi_N + \gamma) = P_L - P_{set} + \frac{|V_N|^2}{|Z_G|}\cos\gamma,$$
$$\frac{|V_N||V_G|}{|Z_G|}\sin(\phi_N + \gamma) = Q_L - \frac{V_{N,0} - |V_N|}{K_V} + \frac{|V_N|^2}{|Z_G|}\sin\gamma.$$

Taking squares of both equations and adding them yields a fourth order equation in $|V_N|$. We choose $|V_N|$ to be the real root closest to 120V. Note that for certain sets of parameters, there may be no steady-state (no real roots).

Having solved for $|V_N|$, we can calculate the steady-state $|I_N|$ and φ from (40), where P_N and Q_N are given in (38) and (39); ϕ_N can be calculated using (41), where P_G and Q_G are given in (42). Finally, according to (4) and (8),

$$P_L + iQ_L = |V_N|^2/Z_L^*, \tag{43}$$

yields the load impedance Z_L.

From V_N and I_N, the inverter internal variables can be computed. For example, V_C and V_P follow from linear equations, f_D and V_D by droop equations, V_N' from the phase of V_N, and (r, θ) from (18) as described in III-F.

A similar calculation applies for opposite droop inverter (12). Equations (38) and (39) now become

$$Q_N = Q_{set}, \tag{44}$$

$$|V_N| = V_{N,0} - K_V(P_N - P_{set}). \tag{45}$$

Along with (40), (41), and (8), we get a fourth order equation in $|V_N|$ that can be solved for the steady-state variables.

APPENDIX B
TRANSIENT MODELS

A. Coordinate Transform

We use two representations of dynamic phasors. The Cartesian coordinates and polar coordinates are related as

$$V_N = |V_N|\angle\phi_N = |V_N|(\cos\phi_N + i\sin\phi_N),$$

Taking differential of both sides yields

$$\begin{bmatrix}\Re\delta V_N \\ \Im\delta V_N\end{bmatrix} = \begin{bmatrix}\cos\phi_N & -|V_N|\sin\phi_N \\ \sin\phi_N & |V_N|\cos\phi_N\end{bmatrix}\begin{bmatrix}\delta|V_N| \\ \delta\phi_N\end{bmatrix}. \tag{46}$$

The linearized inverse transform is given by

$$\begin{bmatrix}\delta|V_N| \\ \delta\phi_N\end{bmatrix} = \frac{1}{|V_N|^2}\begin{bmatrix}|V_N|\Re V_N & |V_N|\Im V_N \\ -\Im V_N & \Re V_N\end{bmatrix}\begin{bmatrix}\Re\delta V_N \\ \Im\delta V_N\end{bmatrix}. \tag{47}$$

B. Droop Controller

Droop controller inputs V_N and I_N first pass through bandpass filters, see [18], with the transfer function,

$$\begin{aligned} T_{\text{bpf}}(s) &= \left(\frac{K_b s}{s^2 + K_b s + (2\pi f_0)^2}\right)^2, \\ V_M(s) &= T_{\text{bpf}}(s + iw_0)V_N(s), \\ I_M(s) &= T_{\text{bpf}}(s + iw_0)I_N(s). \end{aligned} \tag{48}$$

where $w_0 = 2\pi f_0$. Transfer functions in s for time signals change the argument to $s + iw_0$ for dynamic phasors [17]. Similar filtering is done for the transient signals from δV_N to δV_M and from δI_N to δI_M. In steady state, we have $V_N = V_M$ and $I_N = I_M$.

We assume that the power measurement is instantaneous. For the transient model, we linearize the nonlinear relationship (5) around the steady-state values V_N and I_N, resulting in a static 2×4 model of the form

$$\begin{bmatrix}\delta P_N \\ \delta Q_N\end{bmatrix} = \begin{bmatrix}\Re I_M & \Im I_M & \Re V_M & \Im V_M \\ -\Im I_M & \Re I_M & \Im V_M & -\Re V_M\end{bmatrix}\begin{bmatrix}\Re\delta V_M \\ \Im\delta V_M \\ \Re\delta I_M \\ \Im\delta I_M\end{bmatrix}. \tag{49}$$

T_{msr} is obtained by combining (48) and (49).

Linearizing conventional droop equations in (10) yields the transient dynamics

$$\begin{bmatrix}\delta V_D \\ \delta f_D\end{bmatrix} = T_{\text{droop}}\left(\begin{bmatrix}\delta P_N \\ \delta Q_N\end{bmatrix} - \begin{bmatrix}\delta P_{set} \\ \delta Q_{set}\end{bmatrix}\right), \tag{50}$$

$$T_{\text{droop}} = \begin{bmatrix}0 & -K_V \\ -K_f & 0\end{bmatrix}. \tag{51}$$

For opposite droop (12), the linearization has form (50) with

$$T_{\text{droop}} = \begin{bmatrix}-K_V & 0 \\ 0 & -K_f\end{bmatrix}. \tag{52}$$

C. PLL

PLL input is $V_N = |V_N|\angle\theta_N$; the outputs are phasing signal $V_N' = 1\angle\theta_{N'}$, frequency f_M, and amplitude V_M. In the steady-state, the input amplitude is $|V_N|$, the output phase $\theta_{N'} = \theta_N$, and the output frequency is f_0.

The PLL uses PI feedback of the tracking error. Let the transfer function of the PI controller be $2\zeta_p w_p + w_p^2/s$. Then, according to [22],

$$\delta\theta_{N'} = \frac{2\zeta_p w_p s + w_p^2}{s^2 + 2\zeta_p w_p s + w_p^2}\delta\theta_N. \tag{53}$$

Linearized model (47) of the PLL gives the amplitude measurement $\delta V_M = \delta|V_N|$, where $\delta|V_N|$ follows (47). The transient frequency and phase relation is similar to (1), i.e. $\delta f_M = \frac{1}{2\pi}\frac{d}{dt}\delta\theta_{N'}$. Combining this with (53) yields

$$\delta f_M = \frac{s}{2\pi|V_N|^2}\frac{2\zeta_p w_p s + w_p^2}{s^2 + 2\zeta_p w_p s + w_p^2}\begin{bmatrix}-\Im V_N & \Re V_N\end{bmatrix}\begin{bmatrix}\Re\delta V_N \\ \Im\delta V_N\end{bmatrix}. \tag{54}$$

The linearized transfer function from δV_N to $\delta V_N'$ can be found in a similar way using the transformation of the form (46) proceeded by a bandpass filter T_{bpf} in (48) [18].

D. PI Controller

The PLL outputs f_M, V_M and the desired values f_D, V_D from the droop controller are fed into two PI controllers to produce control signals r and θ. In the steady-state, $f_M = f_D$ and $V_M = V_D$. The linearized controller model has the form

$$\delta\theta = \frac{K_{\theta_I}}{s}(\delta f_D - \delta f_M), \tag{55}$$

$$\delta r = \frac{K_{r_I}}{s}(\delta V_D - \delta V_M), \tag{56}$$

where K_{θ_I} and K_{r_I} are I controller gains.

E. Phase Converter

The phase converter transforms the control signals r and θ (in polar coordinates) from the PI controllers to phasor V_P (in Cartesian coordinates) that drives the IGBT switching gates. PLL output V_N' is used to align V_P with the instantaneous phase of the voltage V_N. This can be expressed as

$$V_P = \frac{1}{\sqrt{2}}(r\angle\theta)V_N', \tag{57}$$

where the scale $\frac{1}{\sqrt{2}}$ ensures that V_P is a RMS measurement. Linearizing (18) around the steady-state, we get

$$\begin{bmatrix}\Re\delta V_P\\ \Im\delta V_P\end{bmatrix} = \frac{1}{\sqrt{2}}\begin{bmatrix}r\cos\theta & -r\sin\theta\\ r\sin\theta & r\cos\theta\end{bmatrix}\begin{bmatrix}\Re\delta V_N'\\ \Im\delta V_N'\end{bmatrix} + \frac{1}{\sqrt{2}}\begin{bmatrix}\Re(1\angle\theta\cdot V_N') & -\Im(r\angle\theta\cdot V_N')\\ \Im(1\angle\theta\cdot V_N') & \Re(r\angle\theta\cdot V_N')\end{bmatrix}\begin{bmatrix}\delta r\\ \delta\theta\end{bmatrix},$$

where $\delta\theta$ and δr are the PI controller outputs in (55) and (56).

F. Inverter Gain

The PWM frequency is much higher than the grid frequency f_0. With a proper design of a lowpass filter, only the effect on the grid frequency is important. The model for the variation of δV_P is (K_{inv} is a constant gain).

$$\delta V_C = K_{\text{inv}}\delta V_P,$$

G. Inverter Circuit and Grid Circuit

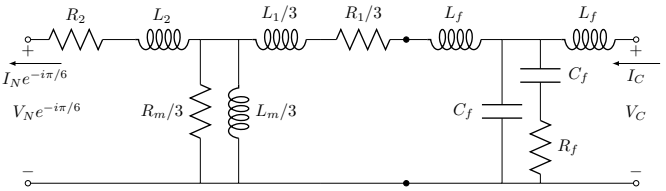

Fig. 13: Inverter circuit.

The inverter circuit includes a lowpass LCL filter and Δ-Y transformer as shown in Figure 13. The filter is composed of two inductances L_f and capacitances C_f in T configuration. The filter follows the design described in [19] and has a shunt resistor in series with a capacitor to suppress high frequencies.

The connection of the inverter circuit and the grid circuit is shown in Figure 2. The grid circuit follows (2), (3), and (4), and the inverter circuit is modeled as a two-port network

$$\begin{bmatrix}V_C\\ I_C\end{bmatrix} = \begin{bmatrix}T_{\text{ickt},11}(s+jw_0) & T_{\text{ickt},12}(s+jw_0)\\ T_{\text{ickt},21}(s+jw_0) & T_{\text{ickt},22}(s+jw_0)\end{bmatrix}\begin{bmatrix}V_N\\ I_N\end{bmatrix},$$

To obtain two-port network transfer functions $T_{\text{ickt},ij}$, where $i,j \in \{1,2\}$, the transfer functions of R, C, and L elements in Figure 13 are combined following KCL and KVL. The dynamic phasor model has transfer function argument changed to $s + jw_0$, where $w_0 = 2\pi f_0$, see [17].

The transient dynamics of the small-signals $\delta V_G(t)$, $\delta V_C(t)$, $\delta V_N(t)$, $\delta I_N(t)$, and $\delta I_G(t)$ becomes

$$\delta V_C = T_{\text{ickt},11}(s+jw_0)\delta V_N + T_{\text{ickt},12}(s+jw_0)\delta I_N, \tag{58}$$

$$(I_N + I_G)\delta Z_L = \delta V_N - (\delta I_N + \delta I_G)Z_L, \tag{59}$$

$$\delta V_G = \delta V_N + \delta I_G Z_G, \tag{60}$$

where we assume that Z_G is a constant. Parameter Z_L may change, for example, due to a change in the load power.

Solving linear equations (58), (59), and (60), we get a linear transfer function from ($\delta\Re V_C$, $\delta\Im V_C$, $\delta\Re V_G$, $\delta\Im V_G$, $\delta\Re Z_L$, $\delta\Im Z_L$) to ($\delta\Re V_N$, $\delta\Im V_N$, $\delta\Re I_N$, $\delta\Im I_N$).

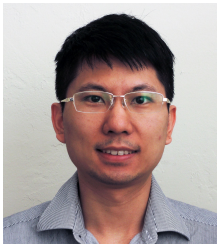

Chung-Ching Chang (S'01–M'14) received the B.S. degree in Electrical Engineering from National Taiwan University, Taipei, Taiwan, in 2003, and M.S. and Ph.D. degrees from Stanford University, Stanford, CA, USA in 2007 and 2013, respectively. His research interests include control, signal processing, optimization, and machine learning, with applications in the smart grid, distributed systems, and computer vision. This work was completed when he was at Stanford. He is now with Google.

Dimitry Gorinevsky (M'91–SM'98–F'06) received a Ph.D. from Department of Mechanics and Mathematics at Moscow (Lomonosov) University in 1986, and a M.Sc. from Moscow Institute of Physics and Technology (Phystech) in 1982. He is a Consulting Professor in Electrical Engineering at Stanford University and a principal of Mitek Analytics LLC consultancy in Palo Alto, CA. In the past, he spent 10 years with Honeywell. He worked on decision and control systems application across many industries. He has authored a book, over 160 papers and 16 patents. Dr. Gorinevsky is a recipient of Control Systems Technology Award, 2002, and Transactions on Control Systems Technology Outstanding Paper Award, 2004, of the IEEE Control Systems Society, Best Paper Award (Senior Award) of the IEEE Signal Processing Society, 2013. He is a Fellow of IEEE.

Sanjay Lall (M'92–SM'06) is Associate Professor of Electrical Engineering in the Information Systems Laboratory and Associate Professor of Aeronautics and Astronautics at Stanford University. He received a B.A. degree in Mathematics with first-class honors in 1990 and a Ph.D. degree in Engineering in 1995, both from the University of Cambridge, England. His research group focuses on control, optimization and signal processing algorithms which occur in a wide variety of electrical, mechanical and aerospace systems. Before joining Stanford he was a Research Fellow at the California Institute of Technology in the Department of Control and Dynamical Systems, and prior to that he was a NATO Research Fellow at Massachusetts Institute of Technology, in the Laboratory for Information and Decision Systems. He was also a visiting scholar at Lund Institute of Technology in the Department of Automatic Control.